Electronic Supplementary Material (ESI) for Journal of Materials Chemistry C.

Supporting Information

Achieving High-performance Narrowband Blue MR-TADF Emitter by Suppressing Isomer Formation and Extending π-conjugate Skeleton

Kaiyuan Di[a], Runda Guo[ac,] *, Yaxiong Wang[a], Yingbo Lv[b], Hanrui Su[a], Qiang Zhang[a], Bing Yang[b] and Lei Wang[a,] *

[a] *Wuhan National Laboratory for Optoelectronics, Huazhong University of Science and Technology, Wuhan, 430074, People's Republic of China.*

[b] *State Key Laboratory of Supramolecular Structure and Materials, Jilin University, Changchun, 130012, People's Republic of China.*

[c]*State Key Laboratory of Luminescent Materials and Devices South China University of Technology, Guangzhou 510640, People's Republic of China.*

Corresponding Author

[*]*Email: wanglei@mail.hust.edu.cn,*

[*]*Email: runda_guo@hust.edu.cn.*

Characterization.

The intermediates and final compounds were confirmed by ^{1}H NMR or ^{13}C NMR spectra on a Bruker-AF301 AT 400 or 600 MHz spectrometer. Thermogravimetric analysis (TGA) was undertaken using a PerkinElmer Instruments Pyris1 TGA at a heating rate of 10 °C min^{-1} from 30 to 600 °C under a nitrogen atmosphere. Mass spectra were recorded on high resolution Fourier-transform mass spectrometer. Differential scanning calorimetry (DSC) was measured under nitrogen on a PE Instruments DSC 2920 unit at a heating rate of 10 °C min^{-1} from 30 to 300 °C. The thermal decomposition temperatures (T_d) were corresponded to 5% weight loss temperatures. The glass transition temperature (T_g) was determined from the second heating scan. The PL spectra and the transient photoluminescence spectra were recorded on an Edinburgh Instruments (FLS 920 spectrometer). The UV-vis absorption spectra were measured on

a Shimadzu UV-VIS-NIR Spectrophotometer (UV-3600) in the wavelength range of 190-1100 nm. The absolute PLQY tests were carried out using a Zolix OmniFluo spectrofluorometer equipped with a calibrated integrating sphere. Cyclic voltammetry was recorded on a computer-controlled EG&G Potentiostat/Galvanostat model 283 at room temperature with a conventional three-electrode system, which consisted of a platinum wire counter electrode, $Ag/AgNO_3$ (0.1 M) reference electrode, and a glassy carbon working electrode of 2 mm diameter. A 0.10 M tetrabutylammonium hexafluorophosphate (*n*-Bu_4NPF_6) solutions in dry dichloromethane and *N*,*N*-dimethylformamide were employed as the supporting electrolyte, and ferrocene was added as a calibrant in the whole measurement.

Device fabrication and measurements.

The used ITO glass substrates, MoO_3, LiF, TAPC, *m*CP, PPF and TmPyPB were commercially available. The devices were fabricated by evaporating organic layers on ITO (20 Ω $square^{-1}$), which were precleaned carefully and treated with oxygen plasma for 5 min. The devices were deposited in the vacuum of 2×10^{-6} Torr. For all of the OLEDs, the emitting areas were determined by the overlap of two electrodes as 0.09 cm^2. The *J*-*V*-*L* of the devices was measured using a Keithley 2400 source meter equipped with a calibrated silicon photodiode. The EL spectra were measured using a PR655 spectrometer. All measurements were carried out at room temperature under ambient conditions.

Calculation details.

The density functional theory (DFT) and timed dependent DFT (TD-DFT) calculations were employed to optimize the ground state and excited state geometries and electronic properties, which were carried out with the B3LYP hybrid functional at the basis set level of 6-31G(d). the spin-orbit couplings (SOC) were calculated by def2-SVP basis set using BDF code.

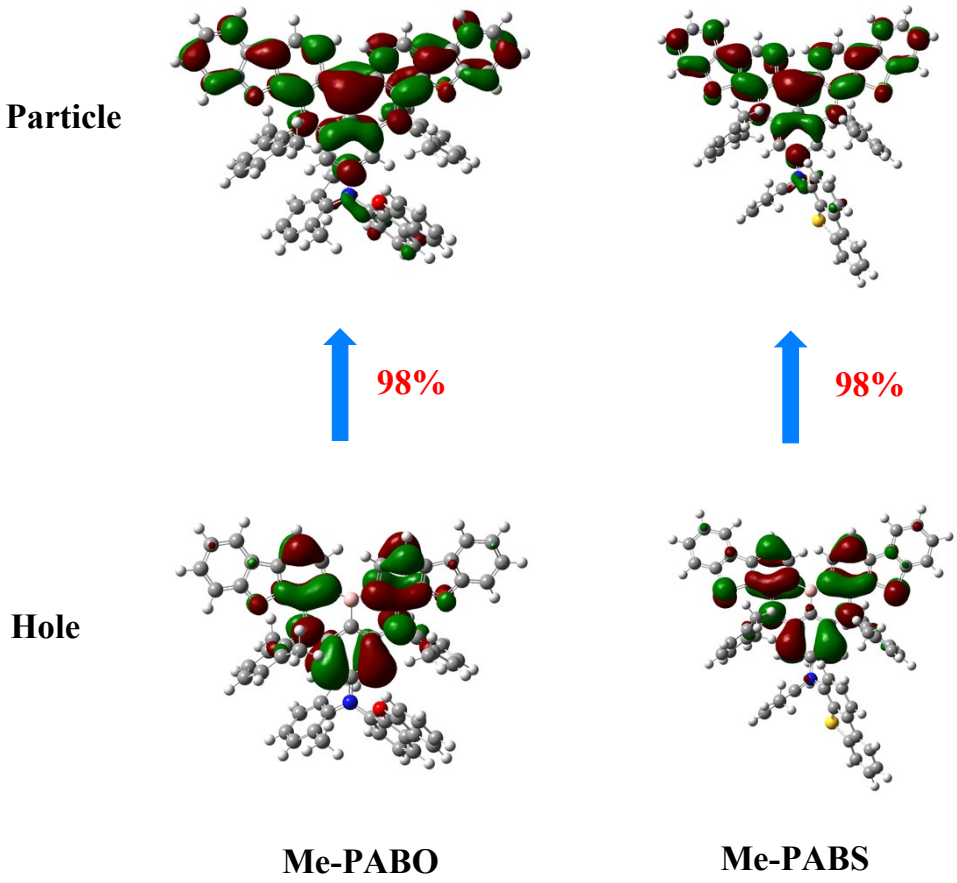

Figure S1. Highest occupied and lowest unoccupied natural transition orbitals (HONTOs and LUNTOs) for the S_1 state of **Me-PABO** and **Me-PABS**.

Table S1 Spin-orbit coupling (SOC) matrix elements between the low lying singlet and triplet excited states of the fluorophores with all values reported in cm^{-1}

SOC	S_1-T_1	S_1-T_2	S_1-T_3
PAB	0.0431	0.8495	0.0115
Me-PABO	0.0464	0.8300	0.3109
Me-PABS	0.0487	0.9400	0.3603

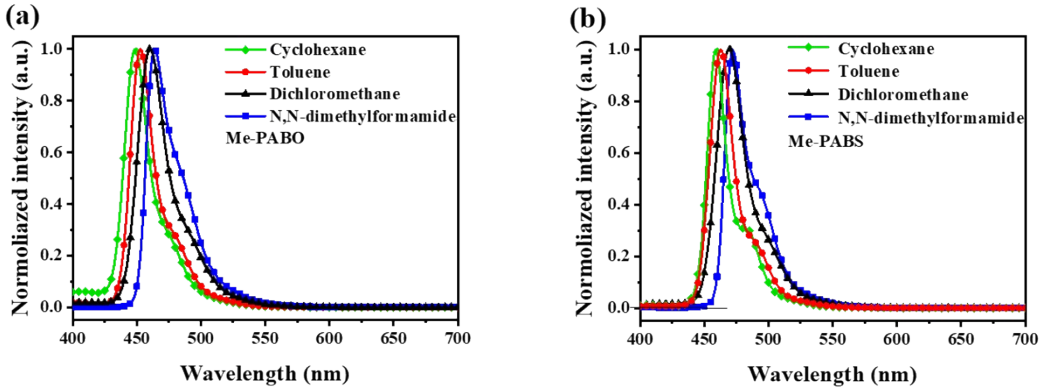

Figure S2. The fluorescence (FL, room temperature) spectra of Me-PABO and Me-PABS in different solvent (1.0×10^{-5} M).

Table S2 The photophysical data of Me-PABO and Me-PABS in different solvents.

Compound	Fluorescence	Cyclohexane	Toluene	Dichloromethane	*N*,*N*-dimethylformamide
Me-PABO	λ^{a}_{em} (nm)	449	453	460	464
	FWHM[b] (nm)	21	21	27	29
Me-PABS	λ^{a}_{em} (nm)	459	463	469	472
	FWHM[b] (nm)	18	21	26	29

[a] The peak wavelength of the PL spectrum. [b] Full width at half maximum.

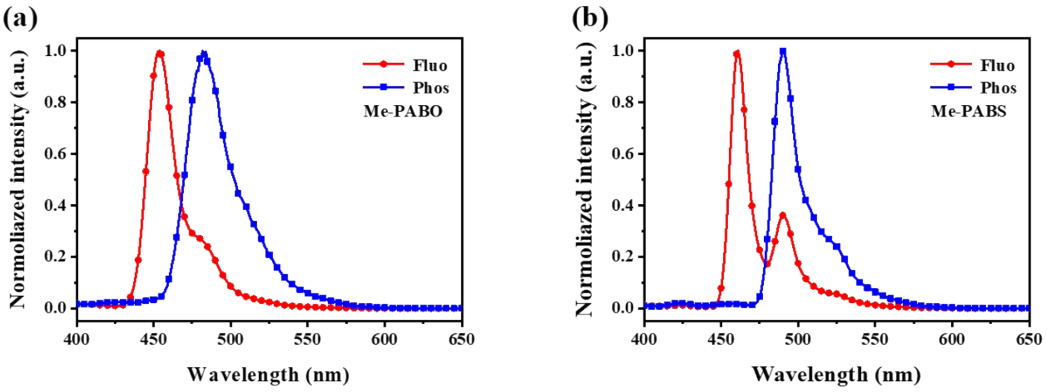

Figure S3. The low-temperature (77K) fluorescence and phosphorescence spectra of Me-PABO and Me-PABS in toluene.

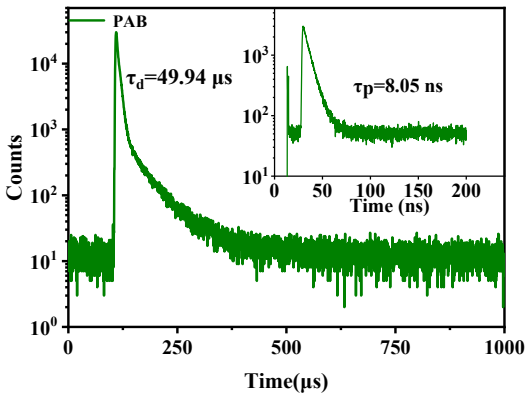

Figure S4 Transient PL decay spectra of PAB doped into PPF films (5 wt%) at room temperature under N_2 (inset: prompt components).

Calculation Formulas for the Photophysical Parameters: The evaluations of exciton dynamic rate constants were calculated by equation S1-S6[1-3]

$k_p = 1/\tau_{PF}$ Equation S1

$k_d = 1/\tau_{DF}$ Equation S2

$k_F = \Phi_{PF}/\tau_{PF}$ Equation S3

$\Phi = k_F/(k_F + k_{IC})$ Equation S4

$\Phi_{PF} = k_F/(k_F + k_{IC} + k_{ISC})$ Equation S5

The total PLQY of the emitter-doped PPF films is high enough. And phosphorescence was not observed at room temperature. Therefore, it is reasonably assumed that 1) $k_r^S \gg k_{nr}^S, k_r^T, k_{nr}^T$ and 2) $k_{RISC} \gg k_r^T, k_{nr}^T$. Where k_r^S and k_{nr}^S are the rate constants for radiative and non-radiative decay from S_1, k_r^T and k_{nr}^T are the rate constants of radiative and non-radiative decay from T_1, respectively. It is experimentally observed that $k_p \gg k_d$(Table.S2), then $k_p \approx k_r + k_{ISC} + k_{RISC}$ and $k_p k_d \approx k_r k_{RISC}$. When $k_{ISC} \gg k_{RISC}$, k_p can be expressed as $k_p \approx k_r + k_{ISC}$, and k_{RISC} is obtained as:

$k_{RISC} = k_p k_d/(k_p - k_{ISC})$ Equation S6

Table S3 The photophysical parameter of PAB, **Me-PABO** and **Me-PABS** (5 wt% doped in PPF).

compound	$\Phi/\Phi_{PF}/\Phi_{DF}$	τ_{PF}(ns)/τ_{DF}(μs)	k_p (10^8 s^{-1})	k_d (10^4 s^{-1})	k_F (10^7 s^{-1})	k_{IC} (10^6 s^{-1})	k_{ISC} (10^7 s^{-1})	k_{RISC} (10^4 s^{-1})
PAB	0.651/0.511/0.140	8.05/49.94	1.24	2.01	6.33	3.41	2.67	2.55
Me-PABO	0.875/0.401/0.474	6.12/61.75	1.6	1.6	6.42	9.12	8.67	3.50
Me-PABS	0.921/0.415/0.506	3.15/39.67	3.17	2.52	13.16	11.29	17.42	5.59

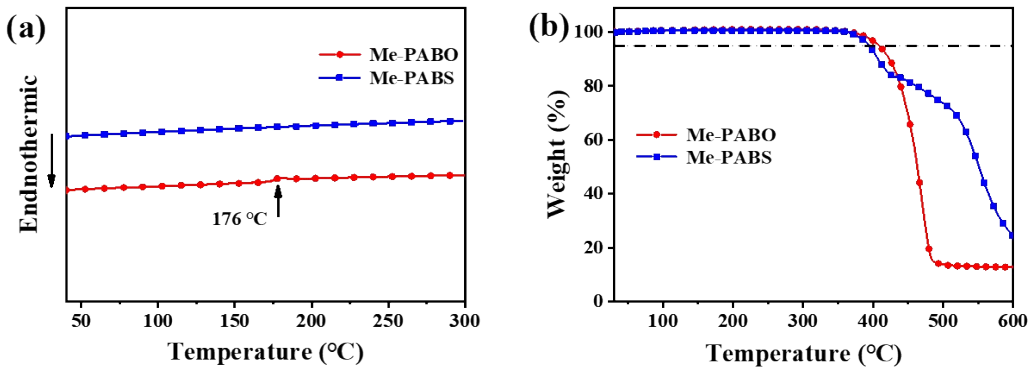

Figure S5. (a) DSC and (b) TGA curves of Me-PABO and Me-PABS.

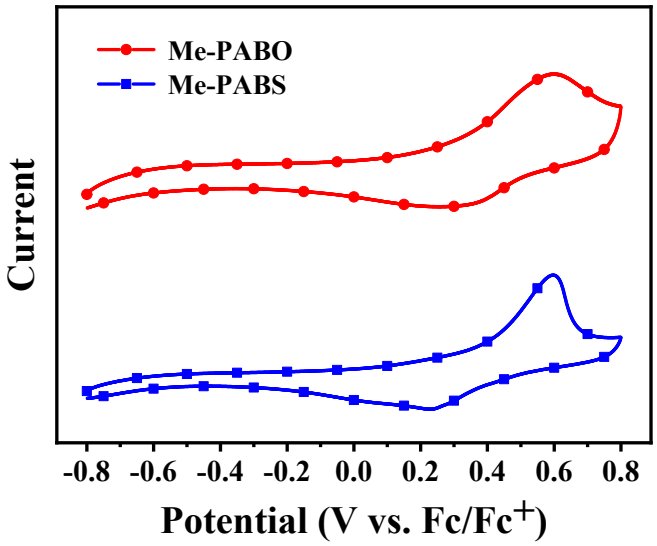

Figure S6. Cyclic voltammogram of Me-PABO and Me-PABS.

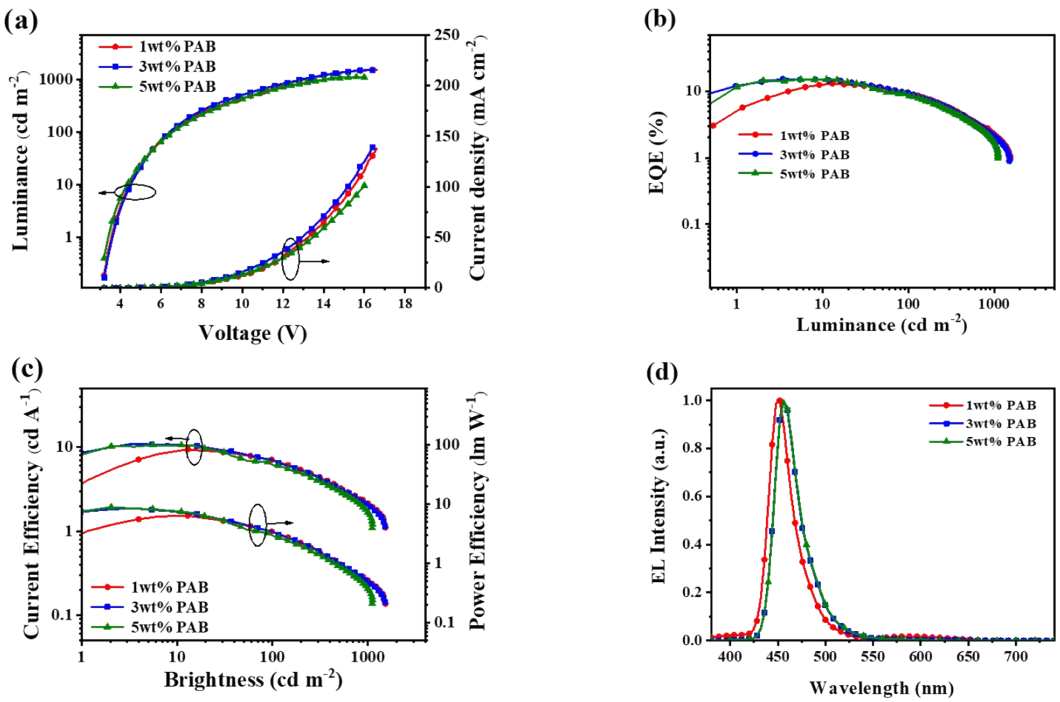

Figure S7. EL characteristics of PAB-based device: (a) Current density-voltage-brightness (J-V-B) characteristics; (b) EQE-brightness curves; (c) current efficiency-brightness-power efficiency curves; (d) normalized EL spectra at 6 V. The device structures were ITO/MoO_3 (10 nm)/TAPC (60 nm)/mCP (10 nm)/PPF: x wt% PAB (20 nm, x=1, 3, 5)/PPF (10 nm)/TmPyPB (30 nm)/LiF (1 nm)/Al (100 nm).

Table S4 The EL performances of OLEDs based on **PAB**.

Compound	V_{on}[a] (V)	L_{max}[b] (cd m^{-2})	CE_{max}[b] (cd A^{-1})	PE_{max}[b](lm W^{-1})	EQE_{max}[b] (%)	λ_{EL}[c] /FWHM[c] (nm)	CIE[d] (x, y)
PAB (1wt%)	3.6	1540	9.43	6.43	13.1	452/30	(0.147, 0.052)
PAB (3wt%)	3.6	1612	10.97	8.61	15.3	456/30	(0.138, 0.075)
PAB (5wt%)	3.4	1651	10.61	8.33	15.1	456/30	(0.138, 0.073)

[a] Voltage at 1 cd m^{-1} (V). [b] Maximum luminance (cd m^{-1}); Maximum current efficiency (cd A^{-1}); Maximum power efficiency (lm W^{-1}); Maximum external quantum efficiency (%). [c] The peak of the EL spectrum; Full width at half maximum of EL spectrum. [d] Commission Internationale de l'Eclairage coordinates.

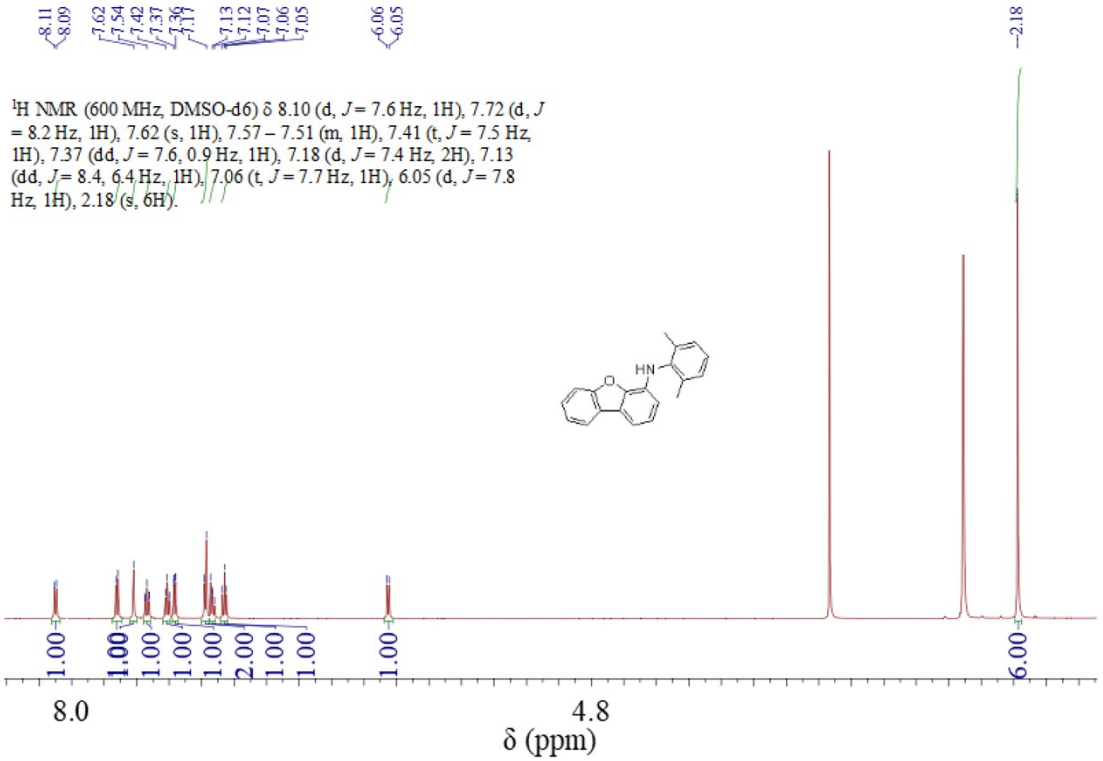

Figure S8. ^{1}H NMR spectrum of 1 in DMSO-d6.

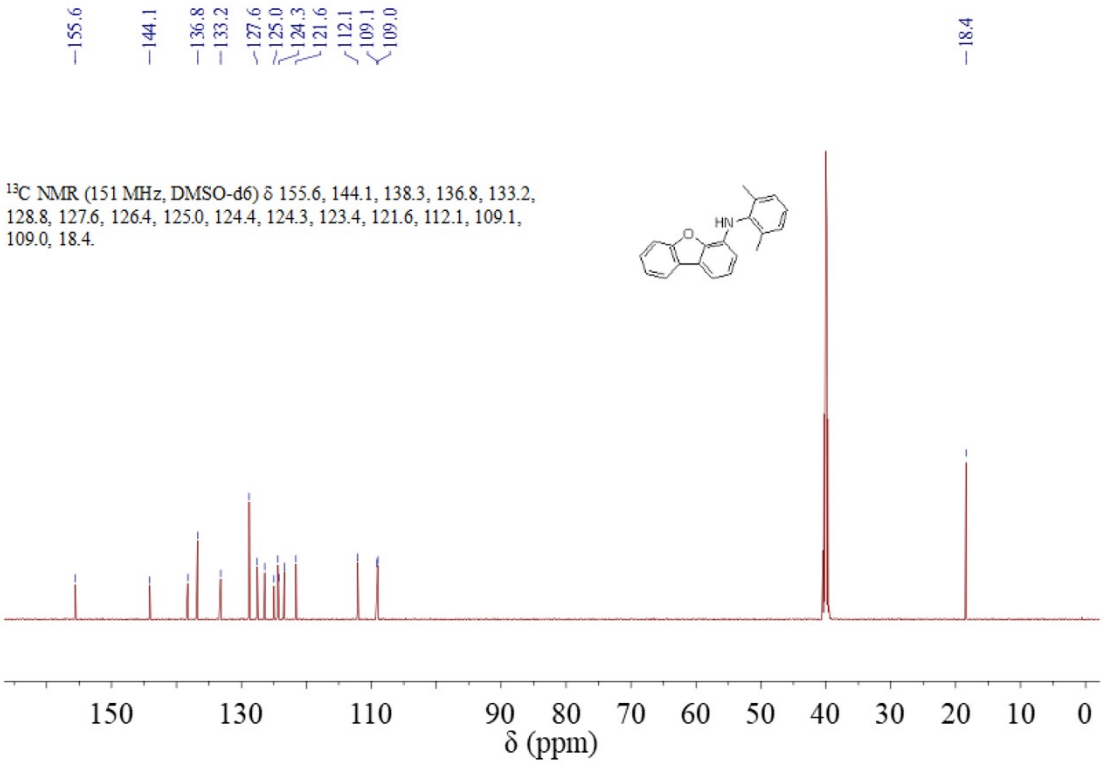

Figure S9. ^{13}C NMR spectrum of 1 in DMSO-d6.

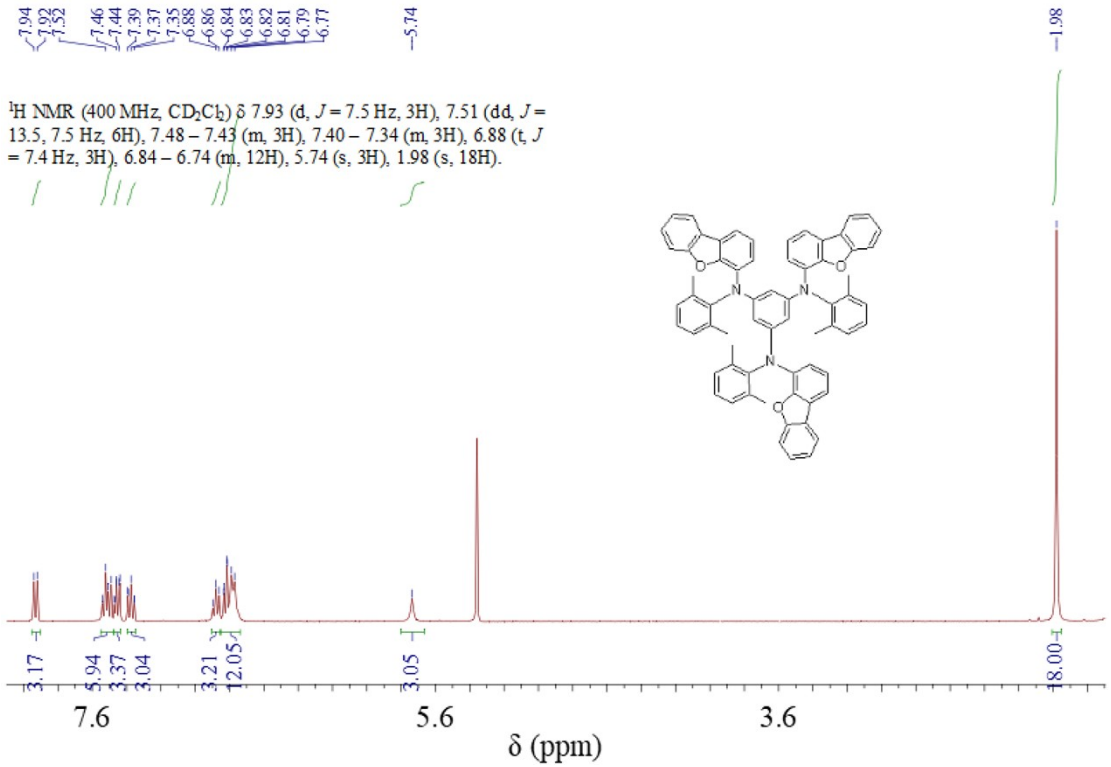

Figure S10. ^{1}H NMR spectrum of 2 in CD_2Cl_2.

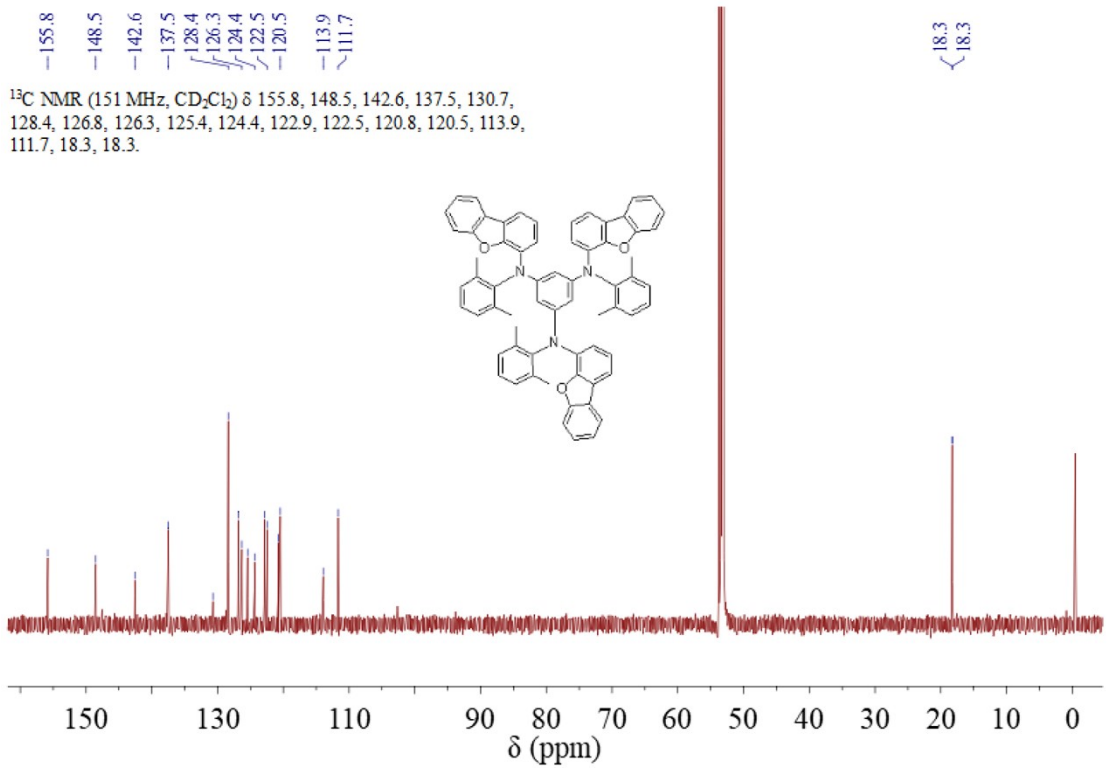

Figure S11. ^{13}C NMR spectrum of 2 in CD_2Cl_2.

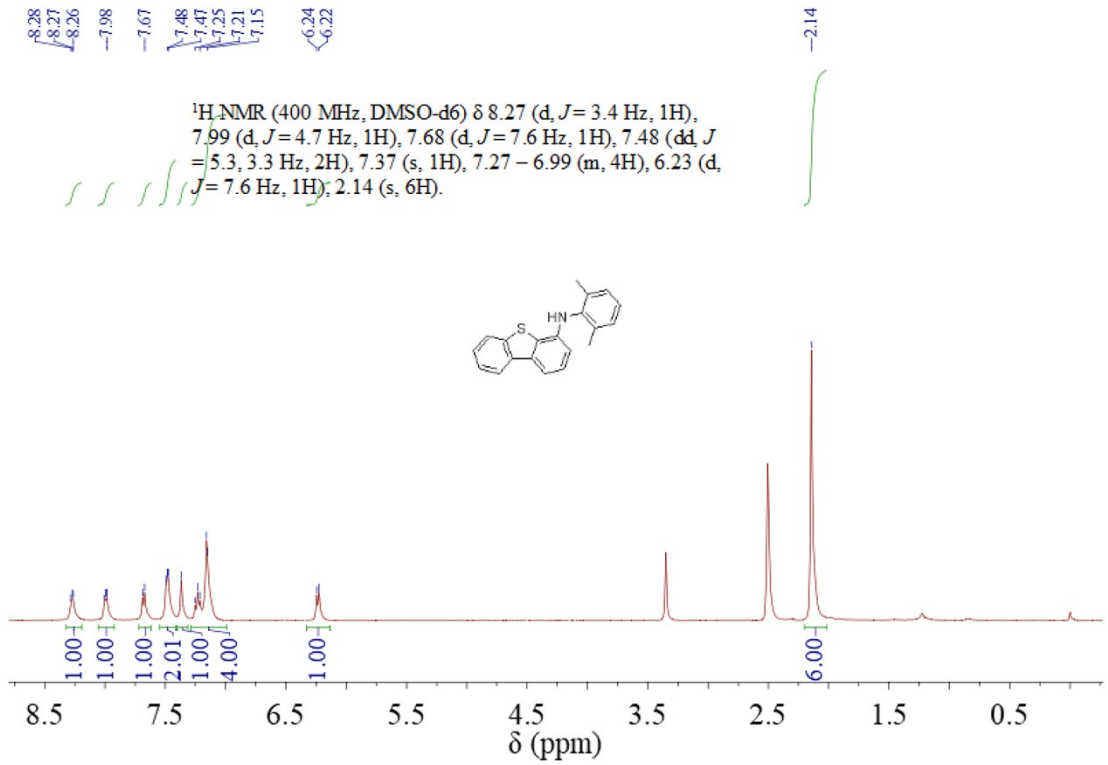

Figure S12. ^{1}H NMR spectrum of 3 in DMSO-d6.

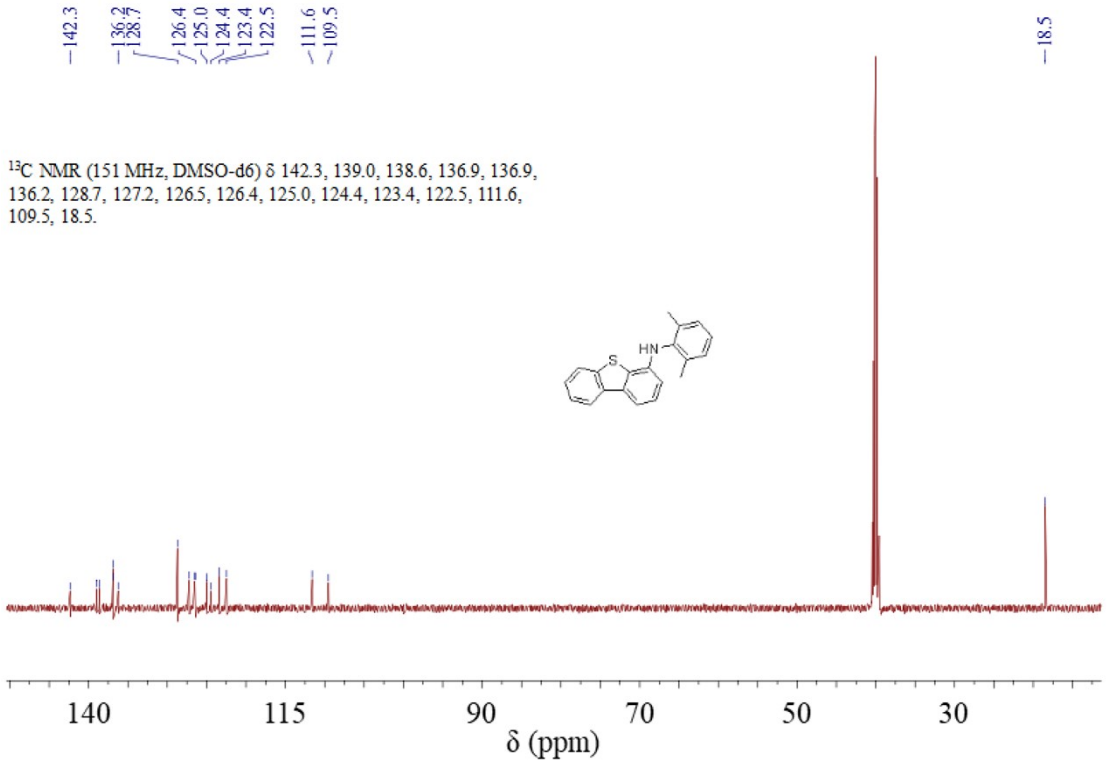

Figure S13. ^{13}C NMR spectrum of 3 in DMSO-d6.

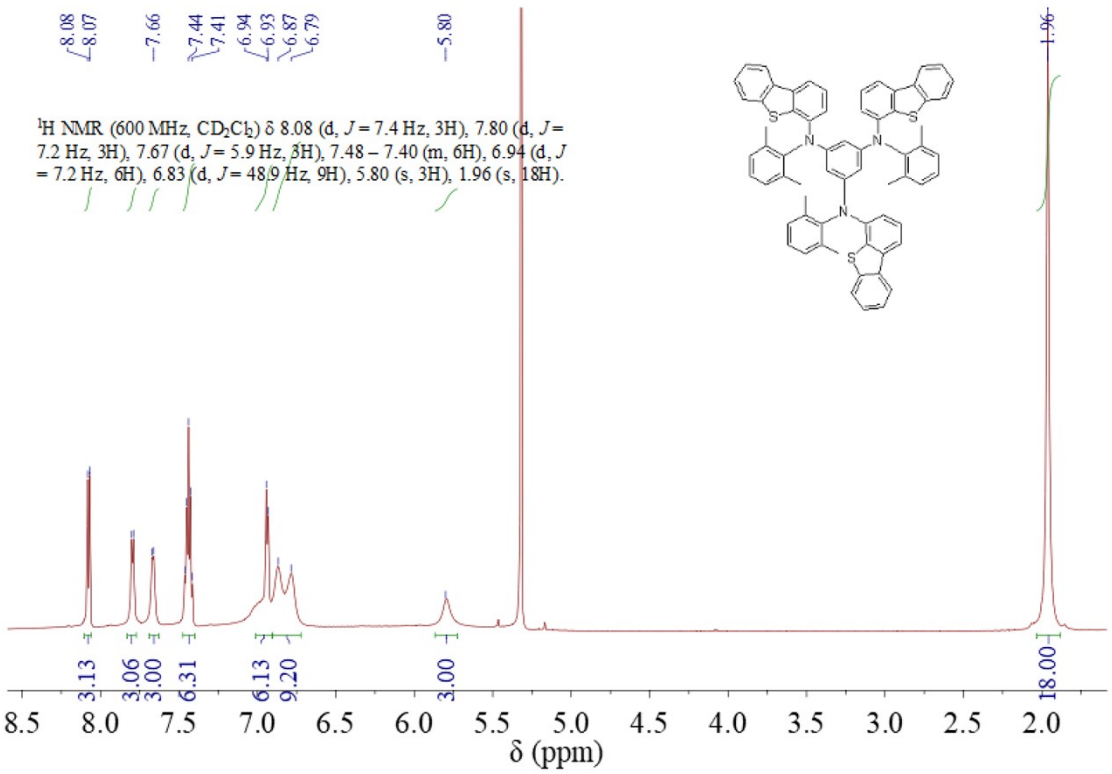

Figure S14. ^{1}H NMR spectrum of 4 in CD_2Cl_2.

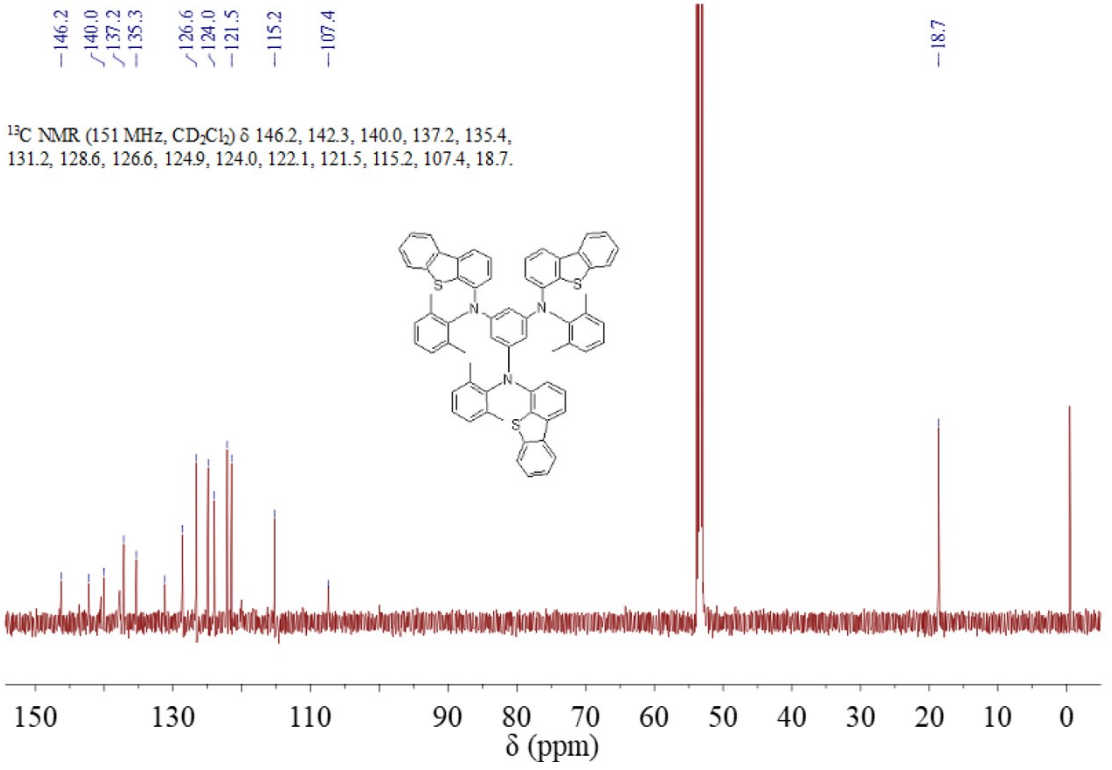

Figure S15. ^{13}C NMR spectrum of 4 in CD_2Cl_2.

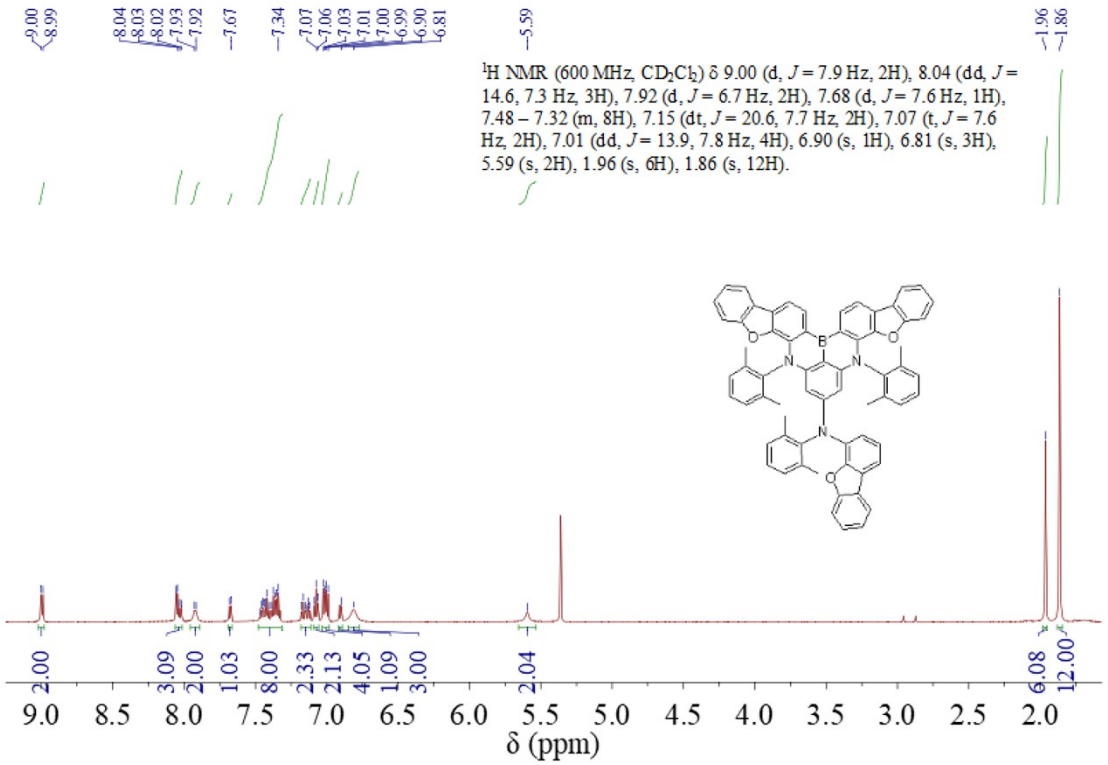

Figure S16. ^{1}H NMR spectrum of Me-PABO in CD_2Cl_2.

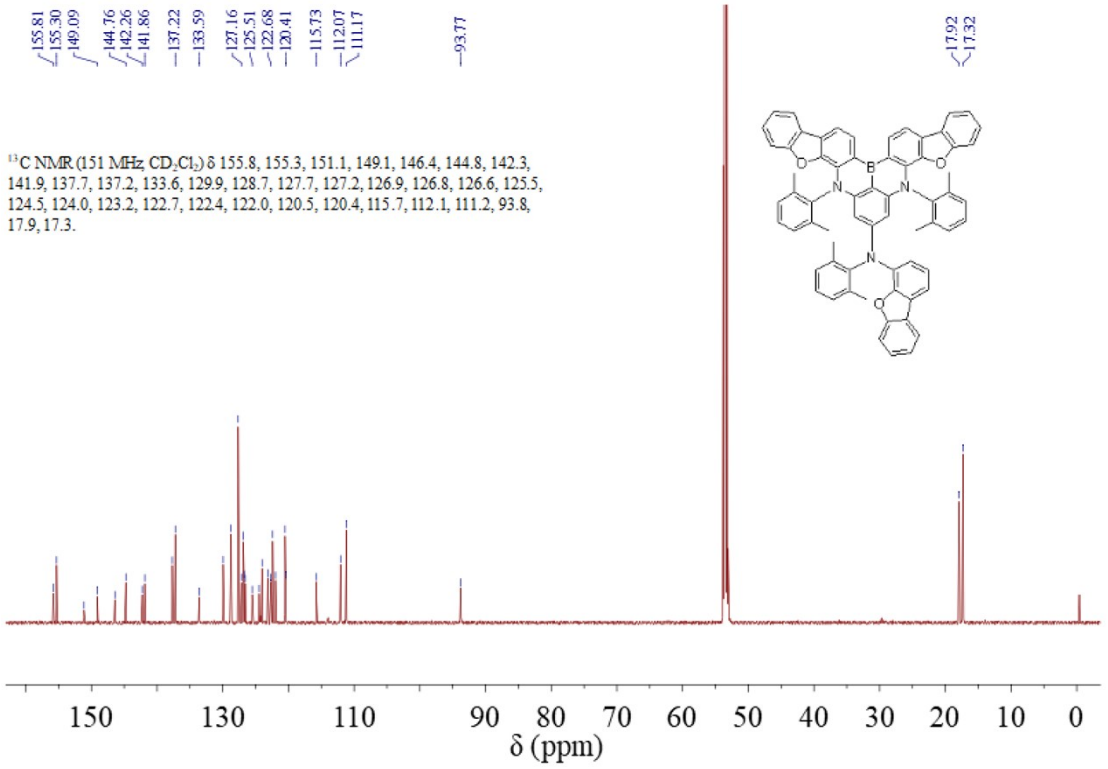

Figure S17. ^{13}C NMR spectrum of Me-PABO in CD_2Cl_2.

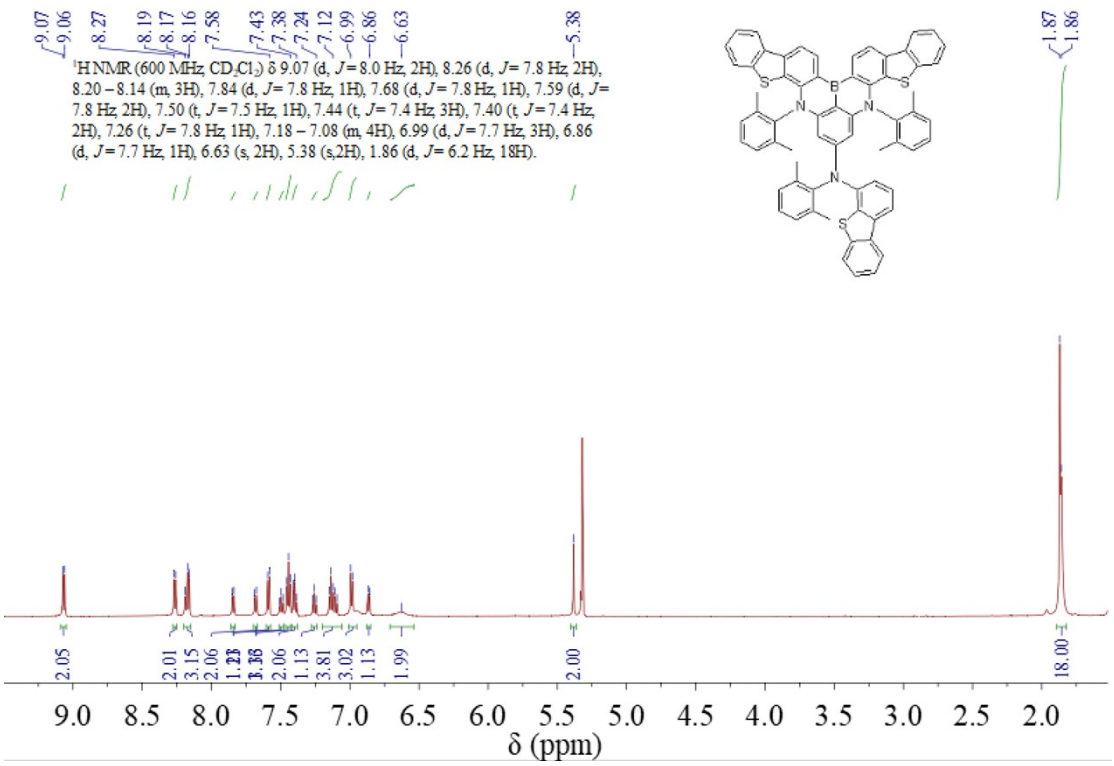

Figure S18. ^{1}H NMR spectrum of Me-PABS in CD_2Cl_2.

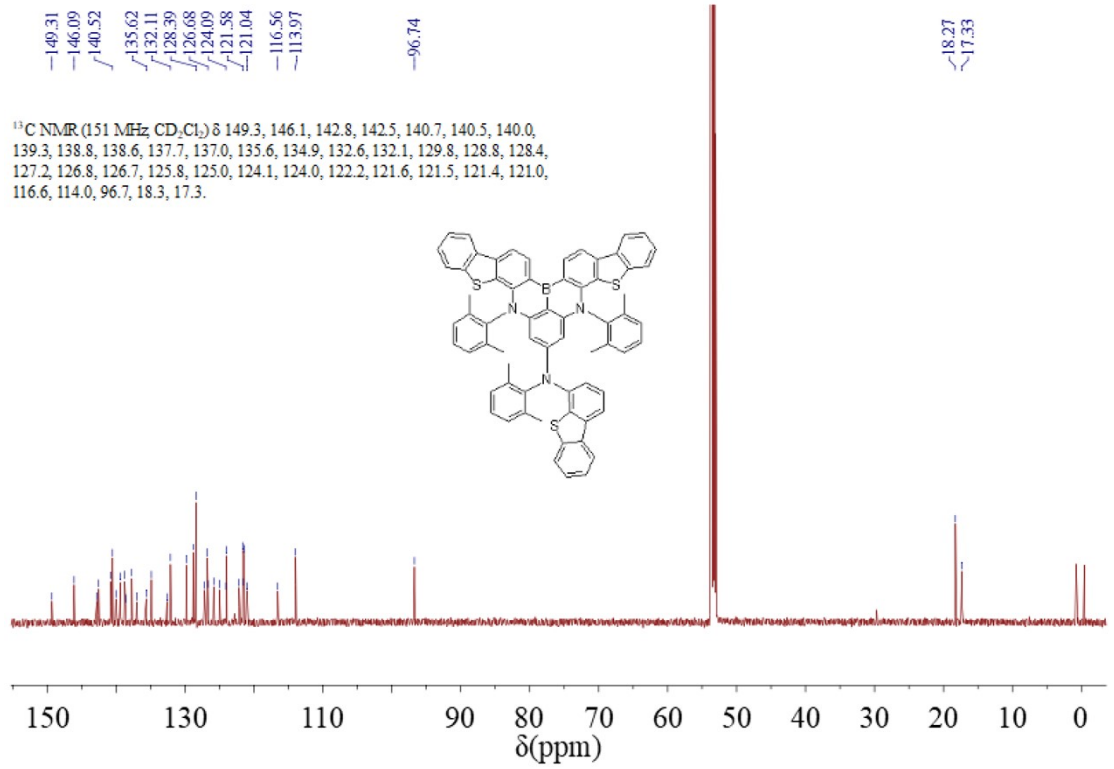

Figure S19. ^{13}C NMR spectrum of Me-PABS in CD_2Cl_2.

References

1. Q. Zhang, H. Kuwabara, W. J. Potscavage, Jr., S. Huang, Y. Hatae, T. Shibata and C. Adachi, *J. Am. Chem. Soc.*, 2014, **136**, 18070-18081.
2. S. Oda, B. Kawakami, Y. Yamasaki, R. Matsumoto, M. Yoshioka, D. Fukushima, S. Nakatsuka and T. Hatakeyama, *J. Am. Chem. Soc.*, 2022, **144** 106-112.
3. Y. Kondo, K. Yoshiura, S. Kitera, H. Nishi, S. Oda, H. Gotoh, Y. Sasada, M. Yanai and T. Hatakeyama, *Nat. Photon.*, 2019, **13**, 678-682.